

Electroweak and Dark Matter Constraints on a Z' in Models with a Hidden Valley

S. Cassel¹, D. M. Ghilencea², G. G. Ross³

Rudolf Peierls Centre for Theoretical Physics, University of Oxford,
1 Keble Road, Oxford OX1 3NP, United Kingdom.

Abstract

We consider current precision electroweak data, Z' searches and dark matter constraints and analyse their implications for an extension of the SM that includes an extra $U(1)'$ massive gauge boson and a particular hidden sector (“hidden valley”) with a confining (QCD-like) gauge group. The constraints on the Z' with arbitrary $Z - Z'$ kinetic mixing coming from direct searches and precision tests of the Standard Model are analysed and shown to lead to a lower limit of 800 GeV on its mass. Renormalisable interactions involving the Z' probe the physics of the hidden valley sector which contains a pseudoscalar dark matter candidate. We find that dark matter constraints place an upper bound on the mass of the Z' of $O(10)$ TeV. A TeV mass scale is needed for the hidden valley states, and the Sommerfeld factor for p-wave dark matter annihilation is found significantly to suppress the allowed parameter space of the model.

¹ e-mail: s.cassel1@physics.ox.ac.uk

² e-mail: d.ghilencea1@physics.ox.ac.uk

³ e-mail: g.ross1@physics.ox.ac.uk

Contents

1	Introduction	1
2	A “hidden valley” extension of the Standard Model	3
2.1	$U(1)'$ physics	5
2.2	Physics of a QCD-like interaction in the hidden valley	6
3	Collider constraints on the Z' boson	10
3.1	Electroweak precision data	10
3.2	Direct Z' searches	12
4	Dark matter constraints	13
4.1	Thermal relic energy density	13
4.2	Hidden valley dark matter candidate	14
4.3	Allowed parameter space and combined mass bounds on Z'	16
4.4	Direct dark matter searches	18
4.5	Indirect dark matter searches	20
5	Conclusions	20
6	Appendix	22
A	GUT embedding and neutrino masses	22
B	Gauge boson eigenstates	23
C	Cross section formulae	24
C.1	Spin 0 dark matter	25
D	Sommerfeld effect	26
D.1	Coulomb potential	29
D.2	Yukawa potential	29

1 Introduction

The Standard Model (SM) has so far proved remarkably successful. With the Large Hadron Collider (LHC) about to start operating, confirmation of its Higgs sector or searches for new physics beyond the SM enter a new, interesting stage, when theoretical ideas and models

advocated over the past three decades face the test of new experimental data. In this paper we consider current precision electroweak data and dark matter constraints and analyse their implications for a rather simple extension of the SM. This consists of the SM and a particular hidden sector that contains matter which interacts under a new confining gauge group, with an extra $U(1)'$ massive boson that couples to SM and hidden sector matter. It was partly motivated by novel LHC signatures and search strategies specific to this type of model. Further interest in this class of models has also been triggered by attempts to explain the excesses in the positron spectrum measured by PAMELA [1] and ATIC [2].

Hidden sectors are a common presence in model building beyond the SM, in models with branes in extra dimensions and in string and supersymmetric models, with many implications such as, for example, supersymmetry breaking [9]. The physics of the hidden sector can in principle be probed by the mediating particles communicating between the hidden and visible sectors. While gravitational interactions are the usual standard mediators, renormalisable operators involving messenger fields such as new gauge bosons, scalars, neutralinos or messenger fermions may also be present. For this latter case, a special class of hidden sectors is that advocated in [3], also called "hidden valley" (HV), where the hidden sector contains some light states in comparison to the energy scale of the mediator. If these light states are able to decay to SM states, the dynamics of the HV models can then produce some novel phenomenology [3, 4, 5, 6, 7, 8], possibly relevant to the LHC. To select search strategies for such new physics, the restrictions that exist on these models from electroweak and dark matter constraints need to be well understood, and this is the main task of this paper.

In this paper we present the constraints on a "hidden valley" extension of the SM with a new neutral gauge boson (Z') dominantly responsible for mediation between the SM and HV sectors. In Section 2 we present the hidden valley model considered, based on the construction of Strassler [3], and define the parameters that will be constrained by current experimental data. In this model the HV matter is confined by a strong (QCD-like) interaction in the hidden sector. The physics of the confining theory is discussed and the spectrum and stability of the HV states determined. In Section 3 we review the constraints on the Z' from electroweak precision data (EWPD) and direct searches, leading to a *lower mass bound* for the mediator. The discussion and conclusions of this section are more general and independent of the physics of the hidden sector. The numerical limits presented allow for the possibility of arbitrarily large kinetic mixing between the hypercharge and $U(1)'$ gauge bosons. So far as we are aware,

these are new results and apply to the case that the SM matter have $O(1)$ $U(1)'$ charges. In Section 4, the consequences of a dark matter candidate in the hidden sector are considered, leading to constraints on the HV dark matter candidate. This will produce an *upper mass bound* on the Z' mediator. We demonstrate that the lower and upper mass bounds can be simultaneously satisfied in a finite region of parameter space that we identify in detail.

The Appendix provides some calculations and results used in the text. In Appendix A additional details on neutrinos masses are provided, while in Appendix B the gauge boson eigenstates are found after the addition of the local $U(1)'$ symmetry to the SM. In Appendix C we list the perturbative gauge boson partial decay rates and spin-0 particle annihilation cross sections used in Section 4. In Appendix D, we discuss non-perturbative corrections to the matrix element for slow moving particles, and present the Sommerfeld factor for p-wave multiparticle states in the presence of Yukawa interactions used for the dark matter relic density calculations.

2 A “hidden valley” extension of the Standard Model

Here we construct a simple extension of the SM based on the construction in [3], which can lead to an interesting non-standard phenomenology. The choice of hidden valley matter content and symmetries is somewhat arbitrary. In addition to the non-supersymmetric SM particle content with right-handed neutrinos $(q_i, u_i, d_i, l_i, e_i, N_i, H)$, four new Weyl fermions $(U_{L,R}, D_{L,R})$ are introduced that make up the hidden sector and a new scalar ϕ is added. The new states are singlets under the SM gauge group G_{SM} . An extra $U(1)'$ gauge group is also assumed under which both SM fields and hidden sector ones are charged, and so by construction the associated gauge boson mediates between the SM and HV sectors.

SM fermions						Scalars		HV fermions			
q_i	u_i^c	d_i^c	ℓ_i	e_i^c	N_i^c	H	ϕ	U_L	U_R^c	D_L	D_R^c
$-\frac{1}{5}$	$-\frac{1}{5}$	$\frac{3}{5}$	$\frac{3}{5}$	$-\frac{1}{5}$	-1	$\frac{2}{5}$	Q'_ϕ	q_+	q_-	$-q_+$	$-q_-$

Table 1: Charges of the fields under the $U(1)'$ that extends G_{SM} .

A simple way to ensure the cancellation of anomalies associated with the $U(1)'$ is to choose the $U(1)'$ charges for the SM fields to be those of the family independent $U(1)_\chi$ subgroup

of a $SO(10)$ GUT, as shown in Table 1. As discussed in Appendix A this model may be considered a low energy realisation of a theory with $SO(10)$ symmetry. However, we do not restrict the analysis to be consistent with $SO(10)$ unification, but this may be recovered as a special case. It follows with the particle content and $U(1)'$ charge assignment in Table 1 that the “un-unified” HV model is still gauge anomaly free. Other $U(1)'$ extensions are possible and will bring different numerical limits on the model parameters compared to those presented in sections 3 and 4. However, as we shall see, the qualitative features of the allowed parameter space found are universal. The vacuum expectation value (vev) of ϕ is responsible for generating a mass for the Z' which we will find is of $O(TeV)$. To allow for right handed neutrinos masses we choose $Q'_\phi = 2$.

One constraint on the hidden valley model which must be satisfied is the upper bound on the number of relativistic degrees of freedom in thermal equilibrium at the time of Big Bang Nucleosynthesis (BBN). This can be satisfied by ensuring that there is a sufficient mass gap for the new states that this model introduces. In the hidden sector, interactions other than $U(1)'$ that are restricted to this sector can also exist. We assume as in [3] that there is a confining $SU(N_v)$ QCD-like interaction with the HV fermions in the fundamental representation and with a confinement scale Λ_{HV} . If $\Lambda_{HV} > \Lambda_{QCD}$, a sufficient mass gap would be provided to satisfy the BBN constraint. This hierarchy can naturally set the mass scale of the HV states to be significantly different from that of SM states, using arguments similar to those in technicolour models. The spectrum of bound states is discussed in Section 2.2.

To allow current masses for the HV fermions via the Higgs mechanism, the condition $q_+ + q_- = -Q'_\phi$ must be satisfied. The field ϕ can then also act as a mediator between the SM and HV sector, via interactions with the SM Higgs of the form $|H|^2 |\phi|^2$. This term produces mass mixing terms between the scalars as well, after breaking the $U(1)'$ and electroweak symmetry. The use of a scalar mediator (also known as the “Higgs portal”) has received recent attention in [11, 12, 13, 14, 39]. In this paper we expect that mediation via the Higgs portal is negligible due to small Yukawa couplings, and the large mass for the ϕ , with the resultant small Higgs- ϕ mixing, making the Z' interactions dominant. Indeed the Higgs portal can be ignored completely in this model if the HV fermions current masses are entirely generated from instanton effects after spontaneous chiral symmetry breaking [15]. Alternatively, if $q_+ + q_- = 0$, mass terms for the HV fermions are unprotected by gauge symmetries and they do not couple directly to the fundamental scalar fields.

2.1 $U(1)'$ physics.

The addition of the $U(1)'$ gauge boson to the SM introduces interesting physics by itself [16, 17]. The discussion here, and in Section 3 for the limits on the Z' from corrections to SM processes, is independent of the details of the hidden sector physics. In the most general case, the Lagrangian can contain a term that leads to kinetic mixing between the Abelian gauge fields $U(1)_Y$ and $U(1)'$:

$$\mathcal{L}_{\text{gauge kinetic}} = -\frac{1}{4} (F_Y^{\mu\nu} F_{Y\mu\nu} + F'^{\mu\nu} F'_{\mu\nu} + 2 \sin \chi F'_{\mu\nu} F_Y^{\mu\nu}) + \text{non-Abelian kinetic terms.} \quad (1)$$

The presence of kinetic mixing and mass mixing terms changes the currents coupling to the gauge fields from that expected in the SM. Since the new scalar, ϕ , is a singlet under G_{SM} , the only unbroken Abelian symmetry after $U(1)'$ and electroweak symmetry breaking (EWSB) is that associated with electric charge conservation, generating the usual structure for electromagnetism. Thus, the physical photon has the same couplings as in the SM, and there is no milli-(electrically)-charged matter in this model at the tree level. After EWSB, an $F'_{\mu\nu} F_{\text{EM}}^{\mu\nu}$ term is generated by loops. For $U(1)'$ couplings in the perturbative regime, this term is negligible for the following analysis.

The currents $J_{A,Z,Z'}$, which include the relevant coupling constants, associated with the canonically normalised gauge boson mass and kinetic eigenstates of the model are related to SM and $U(1)'$ currents $J_{\text{EM},Z}^{\text{SM}}, J'$ as follows (see appendix A for details):

$$\begin{pmatrix} J_A \\ J_Z \\ J_{Z'} \end{pmatrix} = \begin{pmatrix} 1 & 0 & 0 \\ -\cos \theta_w \tan \chi \sin \zeta & \sin \theta_w \tan \chi \sin \zeta + \cos \zeta & \sec \chi \sin \zeta \\ -\cos \theta_w \tan \chi \cos \zeta & \sin \theta_w \tan \chi \cos \zeta - \sin \zeta & \sec \chi \cos \zeta \end{pmatrix} \begin{pmatrix} J_{\text{EM}}^{\text{SM}} \\ J_Z^{\text{SM}} \\ J' \end{pmatrix} \quad (2)$$

$$\tan(2\zeta) = \frac{2\Delta (m_{Z'}^2 - m_W^2 \sec^2 \theta_w)}{(m_{Z'}^2 - m_W^2 \sec^2 \theta_w)^2 - \Delta^2} \quad (3)$$

$$\Delta = \frac{m_W^2 \sin \theta_w}{\cos^2 \theta_w \cos \chi} \left(\frac{2 g' Q'_H}{g_Y} - \sin \chi \right) \quad (4)$$

The ζ angle accounts for the rotation necessary to diagonalise the mass matrix, after kinetic mixing has been removed by a field redefinition. Note that if $\zeta = 0$, the coupling to the physical Z is identical to the SM case, but the Z' coupling still varies with the kinetic mixing χ . It is

therefore not necessary for any SM particles to be charged under the $U(1)'$ for the physical Z' to mediate between the SM and HV sectors as this could be achieved by the presence of kinetic mixing alone. In eq (2), the Weinberg angle is defined as $\theta_w \equiv \arctan(g_Y/g_W)$, and Q'_H in eq (4) is the $U(1)'$ charge of the SM Higgs field. The tree-level mass of the physical Z deviates from the SM prediction:

$$m_Z^2 = \frac{2m_W^2 \sec 2\zeta \sec^2 \theta_w + m_{Z'}^2(1 - \sec 2\zeta)}{1 + \sec 2\zeta} \quad (5)$$

The presence of a local $U(1)'$ symmetry thus affects “low energy” electroweak physics whose parameters have been measured very accurately. The impact of experimental measurements on the mixing parameters, Z' mass, $U(1)'$ coupling constant and matter charges are analysed in detail in Section 3.

2.2 Physics of a QCD-like interaction in the hidden valley

Let us now address the details of the physics of the hidden sector. We consider the case that the HV matter is confined by the strong dynamics of an unbroken gauge symmetry in the hidden sector. We review the behaviour of such QCD-like theories where the elementary matter fields are vector-like pairs of fermions and note some possible differences with SM QCD phenomenology. Here we focus on the lightest composite states since, if stable, these could be the dominant dark matter candidates. The experimental constraints on the hidden valley model with a dark matter candidate are discussed in Section 4.

The Lagrangian with elementary fermions in the fundamental representation of a confining $SU(N_v)$ symmetry ($N_v > 2$) includes the terms:

$$\mathcal{L}_{\text{HV gauge}} = -\frac{1}{4} \mathcal{G}_{\mu\nu}^c \mathcal{G}^{c\mu\nu} - \frac{g^2 \theta_{\text{HV}}}{32\pi^2} \mathcal{G}_{\mu\nu}^c \tilde{\mathcal{G}}^{c\mu\nu} \quad (6)$$

$$\mathcal{L}_{\text{HV fermion}} = \bar{\Psi}_L i \not{D} \Psi_L + \bar{\Psi}_R i \not{D} \Psi_R - \bar{\Psi}_R M \Psi_L - \bar{\Psi}_L M^\dagger \Psi_R \quad (7)$$

where \mathcal{G} is the field strength of the HV-confined gauge field, and chiral multiplets (Ψ) have been formed out of the left- and right-handed Weyl fermions (U, D). Axial rotations can be used to redefine the valley-quark (or “v-quark”) fields, which allows phases to be removed from the v-quark mass matrix. However, a $U(1)_A$ transformation generates non-zero surface terms which contribute to the $\mathcal{G}\tilde{\mathcal{G}}$ term [20]. The effect of choosing a basis where the transformed mass matrix, M' , is real and positive semi-definite, is to shift the θ_{HV} parameter:

$$\theta_{\text{HV}} \rightarrow \theta_{\text{HV}} + \arg \det M \equiv \bar{\theta}_{\text{HV}} \quad (8)$$

While in the SM sector, $|\bar{\theta}_{\text{QCD}}| \lesssim 10^{-9}$, in the present case nothing prevents $\bar{\theta}_{\text{HV}}$ from taking values of order $O(1)$. This term explicitly violates CP symmetry unless $\sin \bar{\theta} = 0$.

The dynamics of the confined matter can be modelled using an effective theory built to possess the conserved and approximate symmetries, as detailed in the following. The kinetic terms of $\mathcal{L}_{\text{HV fermion}}$ are invariant under independent transformations of the left- and right-handed multiplets. Thus, there is a global $U(N)_L \times U(N)_R$ symmetry, where N is the number of HV fermion flavours. The mass terms explicitly break the chiral symmetries down to a vector subgroup. If all flavours have a common current mass, the final symmetry is $U(N)_V$. If the current masses are not degenerate, the final symmetry is $[U(1)_V]^N$.

If there were no fermion masses, the axial symmetry would be spontaneously broken by the v-quark condensate whilst still preserving the vector symmetries. Thus, if there are N' fermions whose current masses are much smaller than the confinement scale, then it is a good approximation to assume that the chiral symmetry of the kinetic term is first explicitly broken to $U(N')_L \times U(N')_R \times [U(1)_V]^{(N-N')}$, and then spontaneously broken to $U(N')_V \times [U(1)_V]^{(N-N')}$. The strong interaction is flavour blind in the limit of zero current masses, so does not spontaneously break the vector symmetry further. The pseudo-Goldstone bosons associated with the spontaneous breaking of the approximate axial symmetry are the analogues of the pions, kaons, eta and eta primed mesons in QCD.

It is convenient to use chiral perturbation theory which is an expansion in terms of the explicit symmetry breaking parameter, M/Λ_{HV} , to model the pseudo-Goldstone boson composite states. The degrees of freedom are parametrised by a field matrix, Σ , which is a function of the N'^2 pseudo-Goldstone bosons:

$$(\Psi_L)_i (\bar{\Psi}_R)_j = -v^3 \Sigma_{ij} \quad (9)$$

where v accounts for the magnitude of the quark condensate and has mass dimension one, and Σ is an $N' \times N'$ matrix. Under a $U(N')_L \times U(N')_R$ transformation, the fields transform as follows:

$$\begin{aligned} \Psi'_L &= L \Psi_L \\ \Psi'_R &= R \Psi_R \\ \Sigma' &= L \Sigma R^\dagger \end{aligned} \quad (10)$$

An exponential representation for Σ is chosen here, defined using the decay constant, f_π :

$$\Sigma = e^{2i\Pi/f_\pi}, \quad \Pi \equiv \frac{\eta'}{\sqrt{2N'}} \mathbf{1} + \pi_a \mathbf{T}_a. \quad (11)$$

The T_a generators are normalised so that $\text{Tr}[T_a T_b] = \delta_{ab}/2$. The pseudo-Goldstone bosons found after spontaneous axial symmetry breaking are pseudoscalars. The effective Lagrangian for Σ , to leading order in M and momentum, is given by [18]:

$$\mathcal{L} = \frac{f_\pi^2}{4} \left[\text{Tr} \left[D^\mu \Sigma^\dagger D_\mu \Sigma \right] + \left(2\mu \text{Tr} [\Sigma M] + \text{h.c.} \right) + \frac{1}{N'} \left(\frac{f_{\eta'}^2}{f_\pi^2} - 1 \right) \left| \text{Tr} [\Sigma^\dagger D_\mu \Sigma] \right|^2 \right] \quad (12)$$

where $\mu = 2v^3/f_\pi^2$. Although the axial $U(1)$ symmetry ($L = R^\dagger$) of the kinetic terms is classically conserved in the limit $M \rightarrow 0$, it is always broken by the triangle anomaly at the loop level. The effect of the anomaly in a $SU(N_v)$ confining theory is vanishing in the limit $N_v \rightarrow \infty$. To describe physics at finite N_v , perturbations can be added with increasing powers of $1/N_v$ [19]. This is important for correctly describing the η' pseudo-Goldstone boson.

The triangle anomaly also controls the $\mathcal{G}\tilde{\mathcal{G}}$ term. It has been shown by 't Hooft [20] that this term can be rewritten as a determinantal interaction of the quark fields, $\det[q\bar{q}]$. The leading order correction in $1/N_v$ to the effective Lagrangian, which explicitly breaks the $U(1)_A$ symmetry, is then given below:

$$\delta_a \mathcal{L} \propto e^{i\theta_{\text{HV}}} \det[\Sigma] + \text{h.c.} \quad (13)$$

The vacuum alignment of the quark condensate in the flavour space, $\langle \Sigma \rangle$, is selected where the potential of the effective theory is minimised. Once this is found, the fields can be expanded about their vevs to determine physical parameters such as the masses and couplings.

Before proceeding further, along this line, let us consider the nature of the dark matter candidates. As discussed later in Section 4.2, the flavoured “valley-pions” (or “v-pions,” π_v) are the dark matter candidates, which is possible since a flavour symmetry can protect them from decay. The pion analogues are the lightest states in this effective theory, with the π_v^0 ($= \pi_3$) being flavour neutral, and π_v^\pm ($\propto \pi_1 \mp i\pi_2$) flavoured. The $\pm, 0$ indices of the v-pions refer to their flavour isospin as they are electrically neutral. It will be shown that the dominant annihilation mechanism of the stable v-pions is via the Z' when $\Lambda_{\text{HV}} \gtrsim 30 m_{\pi_v}$ or if there is a fractional mass splitting of $O(10\%)$ between the (heavier) π_v^0 and the π_v^\pm . In the remainder of this section we show that such a mass splitting is indeed possible.

To first order in M , the v-pion masses are degenerate (neglecting any mass mixing effects):

$$m_{vp}^2 = \mu \sqrt{m_a^2 + m_b^2 + 2 m_a m_b \cos \bar{\theta}_{\text{HV}}} \quad (14)$$

where $m_{a,b}$ are the magnitudes of the HV fermion current masses. This degeneracy is lifted by $O(M^2)$ terms¹:

$$\delta_m \mathcal{L} = \frac{f_\pi^2}{4} \left[(c_1 \text{Tr}[\Sigma M]^2 + c_3 \text{Tr}[\Sigma M \Sigma M] + \text{h.c.}) + 2c_2 |\text{Tr}[\Sigma M]|^2 \right]. \quad (15)$$

To find the masses of the v-pions, only the two lightest flavours need to be considered when mass mixing can be neglected. For an $SU(2)$ flavour symmetry, one of the terms in eq (15) is redundant, since it can be transformed into one of the other terms using a determinant that is not dynamical:

$$\text{Tr}[A^2] = \text{Tr}[A]^2 - 2 \text{Det}[A] \quad (A \text{ is } 2 \times 2 \text{ matrix}) \quad (16)$$

Using this we may absorb the c_3 term into c_1 . With these considerations, one obtains the v-pion masses to $O(M^2)$ below:

$$m_{\pi_v^\pm}^2 \approx m_{vp}^2 + (c_1 + c_2) \frac{m_a^4 + m_b^4 + 4 m_a m_b (m_a^2 + m_b^2) \cos \bar{\theta}_{\text{HV}} + m_a^2 m_b^2 [2 + 4 \cos(2\bar{\theta}_{\text{HV}})]}{m_a^2 + m_b^2 + 2 m_a m_b \cos \bar{\theta}_{\text{HV}}}$$

$$m_{\pi_v^0}^2 \approx m_{\pi^\pm}^2 + \frac{(c_1 - c_2) (m_a^2 - m_b^2)^2}{m_a^2 + m_b^2 + 2 m_a m_b \cos \bar{\theta}_{\text{HV}}} \quad (17)$$

which are correct up to $O \left[c_1 \sin \bar{\theta}_{\text{HV}} \left(\frac{m_a m_b}{m_{\pi_v^0}} \right) \left(\frac{m_a - m_b}{m_a + m_b} \right) \right]^2$ terms. For a discussion on the contributions from instanton effects to pseudo-Goldstone boson masses at $O(M^{N'-1})$, see [21] and references therein. This however does not affect the mass splitting of the v-pions.

The best fit values for the coefficients of the higher order terms in QCD [22] determines $c_i^{\text{QCD}} = 10^{-3} (\mu^2 / f_\pi^2)^{\text{QCD}} \times [-0.6 \pm 0.3, 0.2 \pm 0.3, (0.9 \pm 0.3)(N_v/3)]_i$, ($N_v = 3$ for QCD), where the N_v scaling for c_i follows in the large N_v limit [18]. In our case, if the hidden sector physics can be approximated by a scaled up version of QCD, using eq (14) and (17) with $\bar{\theta}_{\text{HV}} \sim 0$, a 10% mass splitting for the valley-pions would be found if $(m_{a,b}/\mu)^{\text{HV}} \gtrsim O(0.1)$. This can be satisfied with a suitable choice of $m_{a,b}$ ($< \Lambda_{\text{HV}}$). If $\bar{\theta}_{\text{HV}} \sim \pi$, the π_v^\pm fields become massless

¹The degeneracy is also lifted if the bosons interact non-universally with other fields.

in the limit of degenerate quark current masses. However, the π_v^0 field remains massive, so it can be very easy to find a 10% mass splitting in this regime. As mentioned above, this mass splitting plays an important role in the discussion of the dark matter experimental constraints on the model, and we return to these in Section 4.

3 Collider constraints on the Z' boson

In the following we examine the experimental constraints on the parameters describing the $U(1)'$ extension of the SM presented in Section 2, and investigate in particular the bounds on the mass of Z' . To this purpose we consider precision measurements at colliders and direct searches for new neutral gauge bosons. For a Z' mass of $O(100)$ GeV or less, additional constraints are relevant from determination of the muon anomalous magnetic moment [23]. However, for the model considered this does not further restrict the limits presented.

3.1 Electroweak precision data

In the following we use a model independent formalism [24], developed to quantify the deviation of physics from the Standard Model predictions. The parameters ρ, x and y introduced below define the low energy effective Lagrangian with the physical W^\pm and Z integrated out:

$$\mathcal{L}_{\text{eff}} = -\frac{4G_F}{\sqrt{2}g_W^2\sec^2\theta_W} [\sec^2\theta_W J_{W^+}\cdot J_{W^-} + \rho J_z^2 + 2x J_z\cdot J' + y J'^2] + \dots \quad (18)$$

where $J_z = J_{W_3} - \sin^2\theta_* J_{EM}$. The modified Weinberg angle, θ_* , is introduced to account for the extra component of the electromagnetic current that mixing introduces. The experimental determination of the ρ parameter assumes that the non-oblique terms (x, y) are negligible. For the model discussed in Section 2, the non-oblique coefficients x, y presented below are determined at tree level, using eq (2):

$$x = \frac{\rho \sin \zeta \sec \chi}{(\cos \zeta + \sin \theta_w \tan \chi \sin \zeta)} \quad (19)$$

$$y = \frac{x^2}{\rho} \quad (20)$$

As $|\sin \chi| \rightarrow 1$ (maximal kinetic mixing), $|x| \rightarrow \rho \csc \theta_w$. In this limit, the product of the $U(1)'$ coupling and $U(1)'$ charges of SM matter must be very small in order to satisfy the experimental constraints. The tree-level ρ parameter in this model is:

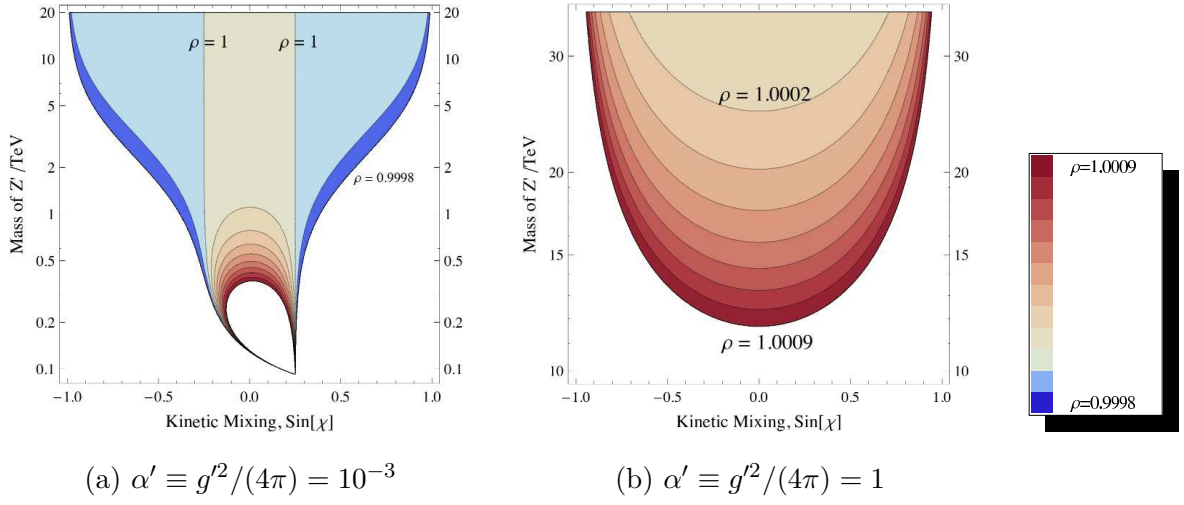


Figure 1: Allowed parameter space for the Z' model given the measurement of the ρ parameter from electroweak precision data, with $Q'_H = 2/5$ (the contours of ρ are spaced every 10^{-4}).

$$\begin{aligned}
\rho &= \frac{m_W^2 \sec^2 \theta_w}{m_{Z'}^2} (\cos \zeta + \sin \theta_w \tan \chi \sin \zeta)^2 \\
&\approx 1 + \frac{m_W^2 \tan^2 \theta_w}{m_{Z'}^2 \cos^2 \chi} \left[\left(2 Q'_H \frac{g'}{g_Y} \right)^2 - \sin^2 \chi \right] + O \left[\frac{m_W^4}{m_{Z'}^4} \right].
\end{aligned} \tag{21}$$

Once radiative effects in the SM are accounted for, the ρ_0 ($\equiv \rho/\rho_{SM}$) parameter, which is sensitive to physics beyond the SM, has been determined by a global fit to the EWPD giving $\rho_0 = 1.0002^{+0.0007}_{-0.0004}$ with the 1σ limits shown [25].

Fig 1 shows the allowed parameter space given this constraint (with $Q'_H = 2/5$) for two values of $\alpha' \equiv g'^2/4\pi$. From that one can easily extract the mass bounds on Z' once we know the values of the kinetic mixing, ρ parameter and α' . Given the definition of the ρ parameter in eq (18), one sees that the limits presented are insensitive to the hidden valley at tree level and also to the SM fermion $U(1)'$ charges. In Fig 1a, the point where the current coupling to the physical Z is identical to the SM case ($\zeta = 0$) is at $\sin \chi \sim 0.25$. The plot demonstrates that any value for $m_{Z'}$ will satisfy the ρ constraint at this point when the tree level result is considered. For small $m_{Z'}$, although not noticeable in Fig 1a, the ‘arm’ of allowed parameter space extending from the opposite sign of $\sin \chi$ does not meet with the straight $\rho = 1$ line (ie there is no ‘hole’ in the allowed parameter space). For large $m_{Z'}$, there is an approximate symmetry in $\chi \rightarrow -\chi$ of the allowed parameter space as suggested by eq (21).

As $g' Q'_H$ is increased, the position of the straight $\rho = 1$ line shifts to larger values for the

kinetic mixing. The ‘arm’ of the allowed parameter space also retracts, and the contours of ρ shift to larger values of $m_{Z'}$. As $g'Q'_H$ is increased beyond $g_Y/2$, the picture of the allowed parameter space then resembles Fig 1b and the contours continue to be shifted to larger values of $m_{Z'}$. It should be noted that when the ρ constraint is very weak, other EWPD measurements provide stronger constraints. However, the strongest constraint on the model introduced in Section 2 is most often from either the ρ parameter or direct searches.

3.2 Direct Z' searches

In this section we consider the mass bounds produced by the Tevatron from searches for new gauge bosons beyond the SM. These can provide a more stringent lower bound for $m_{Z'}$ than electroweak precision data in some cases, and is still present when there is no $Z' - Z_{\text{SM}}$ mass mixing ($\zeta = 0$). Fig 2 shows their experimental limits [26], and the theoretical cross-section for $p\bar{p} \rightarrow Z' \rightarrow e^+e^-$.

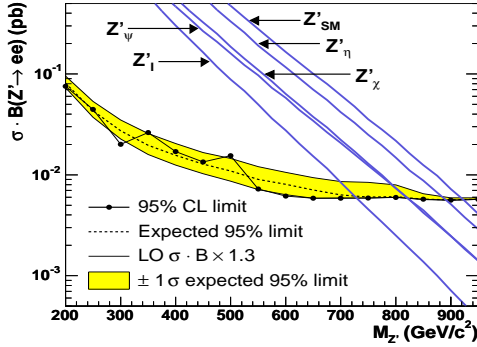


Figure 2: CDF limits on a new spin-1 particle (FERMILAB-PUB-07-367-E)

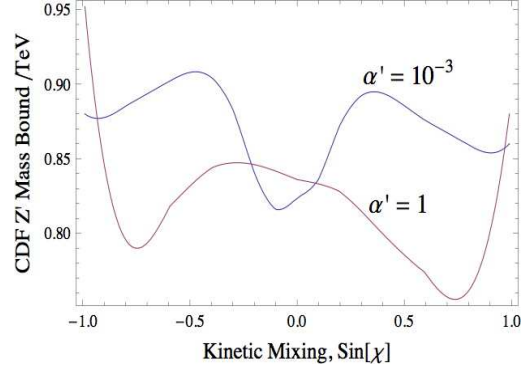


Figure 3: CDF lower mass bound on the Z' in the model presented in Section 2.

The boson labelled Z'_χ has a lower mass bound of 822 GeV. Note that this Z'_χ is the same as Z' introduced in Section 2.1, but with no kinetic mixing and with the $U(1)'$ coupling fixed [27] to $g' = \sqrt{\frac{25}{24}} g_W \tan \theta_w$. It is also assumed that the branching fraction to invisible states is negligible. Relaxing this assumption would reduce the theoretical cross section for producing SM final states, and so reduce this lower bound on the Z' mass. However, it will follow that this is a reasonable assumption for the hidden valley extension considered if the dark matter candidate discussed in Section 4 is the lightest HV state coupling to the Z' , and the SM particles have similar (or greater) order of magnitude $U(1)'$ charges compared to the HV

matter. The constraints on a Z' where the SM particles have no $U(1)'$ charges have been discussed in other papers [28, 29, 30, 31, 32].

The lower bound on the mass of the Z' introduced in Section 2.1 for arbitrary kinetic mixing and negligible decay to HV states is shown in Fig 3. Since the theoretical resonant cross section is controlled by branching fractions, the lower bound on $m_{Z'}$ only varies by $\sim 10\%$ as the (g', χ) parameters vary. For large α' , the ρ constraint is much stronger.

4 Dark matter constraints

Let us now address the dark matter constraints on the model. We first state the method for calculating the thermal relic abundance of a stable particle and discuss what conditions are necessary for a dark matter candidate from the “hidden valley” to contribute significantly to the present day non-baryonic matter energy density. We present limits on the parameters of the hidden valley model from ensuring that dark matter is not overproduced and consider the constraints from direct dark matter searches. We find in particular upper mass bounds on Z' which will be combined with the lower mass bounds of Section 3.

4.1 Thermal relic energy density

During inflation, the reheating may have been sufficient for the Z' mediator to thermalise the SM and HV sectors. If not, the temperatures of the two sectors will be independent, and depend on the relative couplings to the inflaton. We consider the former case with a dark matter candidate from the hidden valley that annihilates into the SM sector.

The thermal relic density of a stable particle is controlled by when this particle leaves thermal equilibrium with its annihilation products (“freeze-out”). This occurs roughly when the thermally averaged annihilation rate of this particle becomes slower than the expansion rate of the universe:

$$n \langle \sigma_{\text{ann}} v \rangle \sim H \quad (22)$$

where n is the number density of the particle freezing out, $\langle \sigma_{\text{ann}} v \rangle$ is the thermally averaged annihilation cross section weighted by the relative velocity, and H is the Hubble constant. The ensemble of frozen-out particles then expand isentropically, allowing the present number of particles in a comoving volume to be calculated. The current contribution to the energy density of the universe can then also be determined. If the particles are non-relativistic at

the time of freeze-out, the thermal average is given by:

$$\langle \sigma_{\text{ann}} v \rangle \approx \frac{x^{3/2}}{2\sqrt{\pi}} \int_0^\infty dv v^2 (\sigma_{\text{ann}} v) e^{-xv^2/4} \quad (23)$$

where $x \equiv m_{\text{DM}}/T$. The annihilation cross section can be calculated perturbatively, however for slow moving dark matter there can be important non-perturbative effects due to interactions before annihilation. This is accounted for by the Sommerfeld factor as discussed in detail in Appendix D and other papers [34, 35, 36, 37, 38, 39, 40]. The temperature at which the freeze-out occurs is determined from eq (22), and is parametrised by the value of x at freeze-out [42]:

$$x_F \approx \ln \left(\frac{[3.85 \times 10^{17} \text{ GeV}] g_{\text{DM}} m_{\text{DM}} \langle \sigma_{\text{ann}} v \rangle_{x_F}}{\sqrt{x_F g_{*s}}} \right) \quad (24)$$

where g_{DM} is the number of degrees of freedom of the dark matter candidate. The g_{*s} parameter is the effective number of relativistic degrees of freedom contributing to the entropy density of the universe. For $T \gtrsim 300 \text{ GeV}$, $g_{*s} = 106.75$ (assuming only Standard Model particles contributing), and at $T = 1 \text{ GeV}$, $g_{*s} \sim 80$. The contribution to the energy density is then given by:

$$\Omega_{\text{DM}} h^2 = \frac{8.6 \times 10^{-11} \text{ GeV}^{-2}}{\sqrt{g_{*s}(x_F)} J(x_F)} \quad \text{where} \quad J(x_F) = \int_{x_F}^\infty dx x^{-2} \langle \sigma_{\text{ann}} v \rangle \quad (25)$$

where the approximation that all annihilations cease after “freeze-out” has not been applied. The “annihilation integral,” $J(x_F)$, accounts for the reduction in particle number after “freeze-out.” The thermal relic will contribute to the non-baryonic matter energy density observed in the universe today. The 5-year data from WMAP [43] suggests that $\Omega_c h^2 = 0.1099 \pm 0.0062$, so the central value will be used as an upper limit for the dark matter contribution to Ωh^2 .

The thermal relic abundance increases as the annihilation cross section is reduced. Thus, whereas the constraints in Section 3 led to small cross sections being preferred for Z' mediated or mixing events, the WMAP constraint will limit how small these cross sections are allowed to be, given a thermal relic from the hidden valley.

4.2 Hidden valley dark matter candidate

For the model discussed in Section 2, there are no flavour changing interactions for the HV fermions. A state with a non-zero “flavour” quantum number is therefore stable. If there are

confining interactions for the HV matter, some of the composite states will be flavour neutral (eg π_v^0) and thus unstable due to the presence of the HV-SM mediator. However, there will also be stable states present (eg π_v^\pm) which are dark matter candidates. The lightest stable states dominate the relic density. Since the last annihilation mechanism to freeze-out controls the relic density, the freeze-out temperatures for the processes below must be evaluated and compared, to determine what the dominant annihilation mechanism is:

- $\pi_v^+ \pi_v^- \rightarrow Z' \rightarrow \text{SM}$

This process freezes-out at a temperature $T_1 \sim m_{\pi_v^\pm}/25$ when dark matter is not overproduced but the annihilation is not close to the Z' resonance (in which case $T_1 \sim m_{\pi_v^\pm}/40$). This was found using the annihilation cross sections to SM products listed in Appendix C. The analysis in the following section assumes that this is the dominant process at freeze-out. For π_v^\pm masses in the range 400 GeV to 40 TeV, the freeze-out temperature is passed at a time between 10^{-13} and 10^{-8} sec. The Z' resonance is at $4m_{\pi_v^\pm}^2 \sim m_{Z'}^2 \sqrt{m_{Z'}^2 + \Gamma_{Z'}^2}$ and this relates the upper mass bounds of the π_v^\pm and Z' presented in Section 4.3.

- $\pi_v^+ \pi_v^- \rightarrow \pi_v^0 \pi_v^0$ (followed by decay to SM products)

This annihilation proceeds via the strong interactions of the hidden sector, and may freeze-out after the Z' mediated annihilation. Using the effective Lagrangian in eq (12), the annihilation cross section is:

$$\sigma_{pp} \sim \frac{36\pi^3}{\Lambda_{\text{HV}}^2} \left(\frac{m_{\pi_v^\pm}^2}{\Lambda_{\text{HV}}^2} \right) \frac{\beta_f}{\beta_i} \quad (26)$$

where the velocities of the initial and final states, $\beta_{i,f}$, account for the phase space. A Sommerfeld enhancement from v-strong or other interactions could significantly raise this cross section further. The freeze-out temperature can be found using eq (24):

$$T_2 \approx m_{\pi_v^\pm} / \left[25 - \ln \left(\frac{\Lambda_{\text{HV}}}{10^6 \text{ TeV}} \right) - 3 \ln \left(\frac{\Lambda_{\text{HV}}}{m_{\pi_v^\pm}} \right) + \ln \langle \beta_f \rangle \right] \quad (27)$$

The thermal average of the π_v^0 velocity is found by integrating over the kinematically allowed phase space, which in the non-relativistic limit gives:

$$\langle \beta_f \rangle \approx \sqrt{\frac{x}{\pi}} \left(\frac{1 - \delta^2}{\delta} \right) e^{-(1 - \delta^2)x/2} K_1 [(1 - \delta^2)x/2] \quad \text{if } \delta < 1 \quad (28)$$

where $\delta = m_i/m_f$, and K_1 is a modified Bessel function of the second kind. If the SM sector does leave thermal equilibrium with the HV before the v-strong interactions freeze-out, the total energy in the hidden sector is reduced by the decay of the flavour neutral v-pion to SM states [3]. The relic abundance of the π_v^\pm is then exponentially suppressed by the ratio of the time of freeze-out and π_v^0 lifetime, which can lead to a negligible contribution to the non-baryonic matter energy density. The π_v^0 lifetime is given by:

$$\Gamma_{\pi_v^0}^{-1} \lesssim \left(\frac{10 \text{ TeV}}{\Lambda_{\text{HV}}} \right)^2 \left(\frac{1 \text{ TeV}}{m_{\pi_v^0}} \right) \left(\frac{m_{Z'}}{10 \text{ TeV}} \right)^4 \times \frac{10^{-20}}{\alpha'^2} \text{ sec} \quad (29)$$

- If the v-pions are nearly degenerate with or heavier than the Z' , the “valley” feature of the hidden sector is lost, but extra annihilation channels can become important for the π_v^\pm dark matter candidate. This situation is beyond the scope of the paper.

The unitarity limit places an upper bound on masses for a thermal relic at $O(10^2)$ TeV [44]. At this limit, we see from eq (27) that the v-strong interactions will freeze-out before the Z' mediated interactions if either $\Lambda_{\text{HV}} \gtrsim 10^3$ TeV or there is phase space suppression due to the π_v^0, π_v^\pm mass difference. If the π_v^0 is heavier than the π_v^\pm , this process is known as a “forbidden” channel [45].

For TeV scale dark matter, we see that $T_2 > T_1$ if either $\Lambda_{\text{HV}}/m_{\pi_v^\pm} \gtrsim 30$ or there is phase space suppression, using eq (27). In the case $\Lambda_{\text{HV}}/m_{\pi_v^\pm} = 8$ (14), the Z' mediated annihilation will freeze-out last if the unstable v-hadrons are at least 10% (5%) heavier than the strongly interacting dark matter candidate. It has been shown in Section 2 that this kind of mass spectrum can easily be realised in the hidden sector and in the following we assume that $T_2 > T_1$ is indeed the case and the dark matter is π_v^\pm .

4.3 Allowed parameter space and combined mass bounds on Z'

The constraints on a spin 0 thermal relic which dominantly annihilates via the Z' are now considered. In this the annihilation cross sections of Appendix C are used, corrected by the Sommerfeld factors detailed in Appendix D. Figures 4 and 5 show the allowed parameter space for the dark matter and Z' respectively, for certain values of $U(1)'$ coupling α' and charge Q , with the SM $U(1)'$ charges as given in Table 1. These plots assume that either the dark matter mass or the Z' mass is a free parameter to scan over, with $m_{\text{DM}} < m_{Z'}$. If either

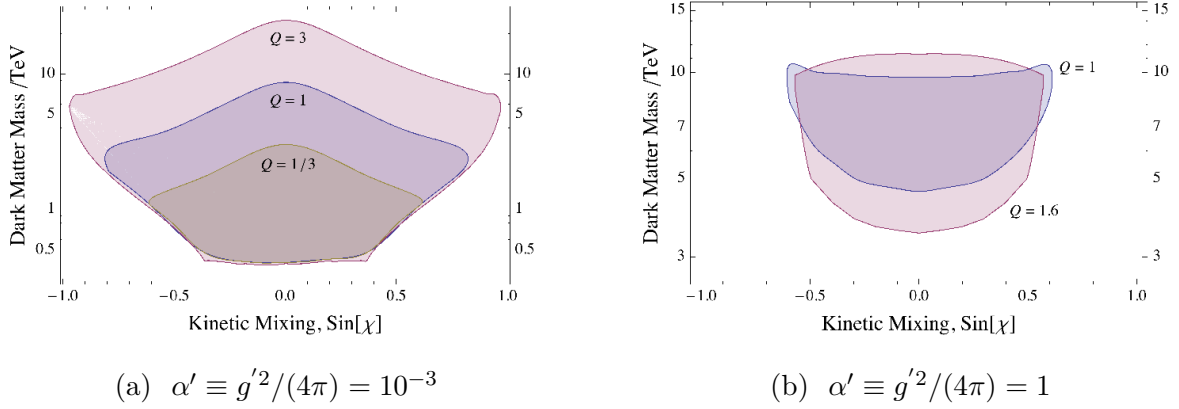


Figure 4: Allowed parameter space for the spin 0 dark matter with $U(1)'$ charge, Q , that dominantly annihilates via a heavier Z' with the SM $U(1)'$ charges given in Section 2.

of these parameters are further constrained by experiment, the parameter space of the other quantity will also be further constrained.

The upper mass bound on the Z' is found when the dark matter annihilation cross section on the Z' resonance is below a critical point, leading to over-production of the DM candidate with respect to the WMAP constraint. The lower mass bound of the dark matter allowed parameter space is controlled by the lower bound of the Z' mass and is the analogue of Lee-Weinberg bound for heavy neutrinos [46]. If the CDF constraint on the Z' mass is relaxed due to a significant branching fraction into HV states, it can be possible for the dark matter to be lighter than that shown in Fig 4 for small kinetic mixing ($|\sin \chi| \lesssim 0.4$).

As $\alpha' Q_{\text{eff}}^2$ increases, where Q_{eff} is the coupling of the π_v^\pm to the Z' which accounts for kinetic and mass mixing using eq (2), the effect of interactions before annihilation (the Sommerfeld effect) becomes much more significant. For spin 0 dark matter, the repulsive interaction between the dark matter particles leads to an exponential suppression of the annihilation cross section. So, the allowed parameter space cannot be made arbitrarily large by increasing the $U(1)'$ charge of the dark matter. When $\alpha' = 1$ and the other parameters are unrestricted, the greatest value for $m_{Z'}$ consistent with the WMAP determination of $\Omega_c h^2$ is ~ 18 TeV. As the coupling of the dark matter to the physical Z' is proportional to $\sec \chi$, the Sommerfeld effect also produces much stronger limits on the amount of kinetic mixing allowed than expected from perturbative calculations.

The upper limits on the masses of the spin 0 dark matter and Z' are found where the

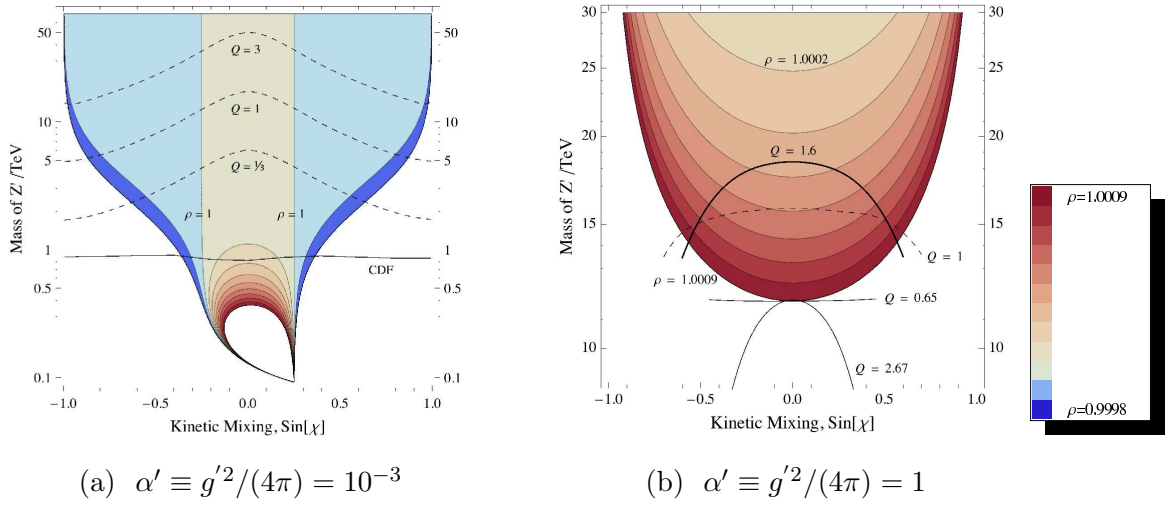


Figure 5: Combined constraints on the Z' with the coloured regions showing the ρ parameter allowed space with 1σ limits determined from electroweak precision data, and lines for the lower mass bound from Z' searches at CDF and upper mass bounds given the presence of a spin 0 dark matter candidate with $U(1)'$ charge, Q , that dominantly annihilates via a heavier Z' . (The contours of the ρ parameter are spaced every 10^{-4}).

dark matter candidate saturates the non-baryonic matter energy density, $\Omega_c h^2$. If a separate particle is found at the LHC, which contributes to $\Omega_c h^2$, the allowed parameter space of the HV dark matter candidate and Z' will be reduced. However, if the annihilation cross section of the HV dark matter has been underestimated, the upper limits are raised. This could be the case from having neglected annihilation products involving supersymmetric SM states.

It is also possible for the HV dark matter to dominantly annihilate through the physical Z , due to kinetic and mass mixing. This does not change the bounds on the physical Z' mass, but does sometimes allow a very narrow region of parameter space for the dark matter around the Z resonance, $m_{\text{DM}} \sim m_Z/2$. This has not been shown in the plots.

4.4 Direct dark matter searches

This section considers the constraints from direct dark matter searches on the HV dark matter candidate. There are numerous experiments which have looked for recoils of nuclear matter due to collisions with dark matter. There have not been any signals observed, except for an annual modulation in the DAMA experiment which prefers light dark matter. The dark matter in this model is too heavy to explain the DAMA signal, so the upper limits on the

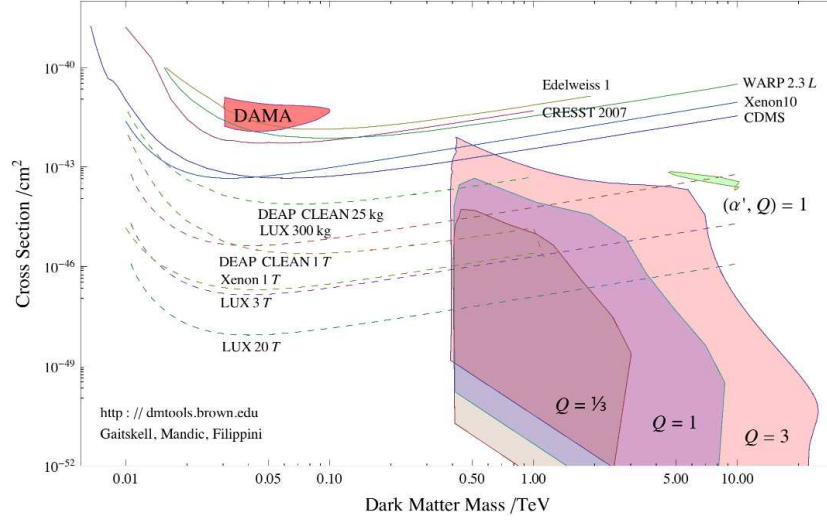


Figure 6: Spin independent cross section for the dark matter scattering off a proton ($\alpha' = 10^{-3}$ apart from green region where $\alpha' = 1$)

scattering cross sections from the other experiments are considered. The current and projected experimental limits are shown in Fig 6 with solid and dashed lines respectively. These cross section limits assume a local dark matter density of $\sim 0.3 \text{ GeV cm}^{-3}$ and mean velocity of $\sim 220 \text{ km s}^{-1}$. If the dark matter candidate does not saturate the non-baryonic matter energy density, then the experimental limits are weakened.

Fig 6 also shows the theoretical prediction from scans of the allowed parameter space, as given in Section 4.3. For the allowed dark matter masses, the Sommerfeld effect is negligible for these calculations. This is because the Z' is much heavier than a proton so the interaction is screened to a small distance compared to the characteristic scattering length scale.

For a certain choice of parameters, the effective vector coupling of the proton to the Z' is zero. In the neighbourhood of this region, the dominant spin independent scattering occurs via the Z . Since the dark matter only gains milli- Z -charges from mixing, the cross section is suppressed. The vast majority of parameter space gives a theoretical cross section within a factor of 10 of the upper boundaries for the regions shaded in Fig 6. It will be unlikely that all experiments use atoms for the dark matter to scatter off that are in the special region of parameter space that allow the very small cross sections.

4.5 Indirect dark matter searches

In this section, we briefly review the prospects for indirect detection of the HV dark matter candidate. There are searches for signals of dark matter annihilation or decay in our galactic neighbourhood. For the latter, the lifetime of the dark matter candidate should be greater than the lifetime of the universe in order for there to be a significant energy density currently present in the universe. Some possible signals include highly energetic photons, neutrinos and antimatter subject to a propagation dispersion relation. The stability of the HV dark matter candidate was inferred by the presence of a flavour symmetry. However, gravity is flavour blind and so we expect Planck suppressed operators to break this symmetry and mediate decay of the π_v^\pm . As for dark matter annihilation signals, since the average velocity of cold dark matter in the galactic halo is of $O(10^{-3})$, the Sommerfeld suppression for the v-pions to annihilate via the Z' strongly reduces the cross section. This results in a negligible signal for current experimental detectors. For dark matter that aggregates inside stars, large planets or dwarf satellite galaxies where the velocities are $O(10^{-5})$, the annihilation signal is even further suppressed. Thus for the repulsive interaction considered here the prospects for indirect dark matter searches are poor, in contrast to the case considered in [39] that for an attractive interaction between the dark matter candidates, these objects can provide a much more favourable source for dark matter annihilation signals.

5 Conclusions

We considered experimental electroweak and dark matter constraints on a simple extension of the SM with an additional $U(1)'$ massive gauge boson and a particular type of a hidden sector (“hidden valley”) with a confining, QCD-like gauge group and hidden valley matter charged under the new $U(1)'$. As a result the SM and hidden valley sectors communicate via renormalisable operators involving Z' as a messenger, which can then probe the physics of the hidden valley sector. The latter can also provide a dark matter candidate. Combined electroweak and dark matter constraints placed both lower and upper bounds on the mass of Z' and these were studied in detail.

We found from corrections to the ρ parameter in electroweak precision data and direct searches a lower limit on the Z' mediator mass of $O(1\text{-}10\text{ TeV})$ depending on the $U(1)'$ coupling constant and kinetic mixing parameter. This result followed when there is a negligible Z'

partial decay rate to HV states and $O(1)$ $U(1)'$ charges for the SM matter. This limit does not require the presence of a hidden valley, as it would similarly apply for a pure $U(1)'$ extension to the SM. In addition, it was demonstrated that the kinetic mixing of the $U(1)'$ and hypercharge gauge bosons is not restricted to be small by current observations.

We also found a dark matter candidate in the strongly interacting hidden valley that could saturate the present day non-baryonic matter energy density. If the spin 0 HV thermal relic dominantly annihilates via the Z' , and the $U(1)'$ charges of the SM and HV states are of similar magnitude, there is an upper bound on the Z' mass of $O(10)$ TeV and restrictions on the amount of kinetic mixing allowed. Although the upper limit is beyond the reach of the LHC [29, 33], a large proportion of the parameter space will be tested. Detection of an alternative candidate to contribute to the dark matter density at the LHC could forbid the presence of this HV thermal relic. The lightest HV state was found to annihilate close to the Z' resonance, restricting it to have an $O(\text{TeV})$ mass. Future direct dark matter searches will also significantly probe the currently allowed dark matter parameter space.

The inclusion of the Sommerfeld effect for p-wave annihilations of the spin 0 dark matter via a spin 1 state brought a significant change to the annihilation cross section. This constrained the parameter space much more than perturbative calculations would have suggested.

If the lightest HV states are $O(\text{TeV})$ and the model discussed is realised, then extra signals containing highly energetic SM decay products of HV states may be observed in collider detectors. The pseudoscalar π_v^0 state would preferentially decay to top quarks, gauge bosons and Higgs fields, and the LHC / Tevatron would see low multiplicity events. There would be insufficient energy and resolution to see the influence of the non-pseudo-Goldstone boson states. In alternative hidden valley scenarios, the phenomenology may be different and further study is important to identify how such models and their collider signals can be constrained.

Acknowledgements

This work was partly supported by the EU contract MRTN-CT-2006-035863. SC is supported by the UK Science and Technology Facilities Council (PPA/S/S/2006/04503). We thank John March-Russell, Subir Sarkar and Stephen West for interesting discussions and suggestions, Richard Gaitskell and Jeffrey Filippini for providing the aggregated data sets of experimental limits from direct dark matter searches and Jihn E. Kim for a clarifying discussion.

6 Appendix

A GUT embedding and neutrino masses

We provide here further details to the discussion in Section 2 to show how neutrino masses can be generated in the model considered. The model discussed may be considered a low energy realisation of a theory with $SO(10)$ symmetry if the SM Higgs field is part of a **10**, **120** or **$\overline{126}$** representation of $SO(10)$, and the non-SM states have quantised $U(1)'$ charges, $q_{\pm}, Q'_{\phi} = 0, \pm 1$, or ± 2 , also forming parts of $SO(10)$ multiplets. The missing states of these $SO(10)$ multiplets can have masses of the $SO(10)$ unification scale depending on the mechanism that breaks this symmetry.

To generate a large Majorana mass for the right-handed neutrino via the Higgs mechanism we choose $Q'_{\phi} = 2$, and so if unification is desired ϕ must belong to a **$\overline{126}$** representation, which may be the multiplet H is embedded in. The vacuum expectation value of ϕ is also responsible for generating a mass for the Z' which we will find is $O(\text{TeV})$ scale. The neutrino mass matrix for one SM family is of the form:

$$\begin{pmatrix} \nu & N^c \end{pmatrix} \begin{pmatrix} 0 & y_{\nu} \langle H \rangle \\ y_{\nu} \langle H \rangle & \lambda \langle \phi \rangle \end{pmatrix} \begin{pmatrix} \nu \\ N^c \end{pmatrix} \quad (\text{A-1})$$

The relation of the scalar vevs to gauge boson masses and couplings is given in Appendix C. For λ of $O(1)$, the heavier neutrino has a mass similar to or heavier than the Z' boson, and for a phenomenologically acceptable mass of $O(eV)$ for the light neutrino, the Yukawa coupling leading to the Dirac mass term must be small, $y_{\nu} \sim 10^{-5}$. This is not much smaller than the electron Yukawa coupling. However, if one wants to avoid the introduction of such a coupling, a Z_2 symmetry may be introduced as suggested in [3] with only the N_i fields having odd parity (in this case the N_i fields are dark matter candidates). This assignment is discrete anomaly free if heavier states with odd parity have been integrated out [10], and it forbids the Dirac mass term. A Majorana mass could be generated for the left-handed neutrinos by a $G_{\text{SM}} \times U(1')$ invariant dimension 6 operator, $LLHH\phi^*/M_{\star}^2$. If this operator is responsible for the light neutrino masses, it suggests that the scale of new physics which leads to lepton number violation is $M_{\star} \sim 10^8 \text{ GeV}$. Figure A-i shows some mechanisms for generating this dimension 6 operator.

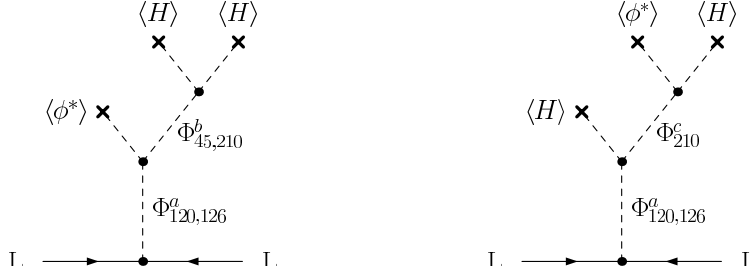


Figure A-i: Some Feynman diagrams that lead to an effective Majorana mass for the SM left-handed neutrinos after integrating out heavy scalar states, Φ . The “X,Y” label on $\Phi_{X,Y}$ indicates that this scalar can be considered as part of an **X** or **Y** representation of $\text{SO}(10)$. The Φ^a field has the representation $(\mathbf{1}, \mathbf{1})(1, -\frac{6}{5})$ under $\text{SU}(3) \times \text{SU}(2) \times \text{U}(1)_Y \times \text{U}(1)_\chi$, Φ^b is $(\mathbf{1}, \mathbf{1})(-1, -\frac{4}{5})$, and Φ^c is $(\mathbf{1}, \mathbf{2})(-\frac{1}{2}, \frac{8}{5})$.

B Gauge boson eigenstates

Here we provide additional details to the discussion in Section 2.1, by computing the gauge boson eigenstate fields in the presence of various mixings present. The kinetic mixing in

$$\mathcal{L}_{\text{gauge kinetic}} = -\frac{1}{4} (F_Y \cdot F_Y + F' \cdot F' + 2 \sin \chi F' \cdot F_Y) + \text{non-Abelian kinetic terms.} \quad (\text{B-1})$$

is removed by the redefinition:

$$\begin{pmatrix} B_\mu \\ B'_\mu \end{pmatrix} = \begin{pmatrix} 1 & -\tan \chi \\ 0 & \sec \chi \end{pmatrix} \begin{pmatrix} \tilde{B}_\mu \\ \tilde{B}'_\mu \end{pmatrix} \quad (\text{B-2})$$

where B_μ is the SM hypercharge boson and B' is the $U(1)'$ gauge boson. After this, \tilde{B}_μ and \tilde{B}'_μ have canonical kinetic terms. Under this transformation ($\mathbf{b} = \mathbf{C} \tilde{\mathbf{b}}$) the source terms for the gauge fields in the Lagrangian, $\mathbf{b}^T \mathbf{j}$, must be invariant, and this fixes the relation between new (“tilded”) and original currents: $\tilde{\mathbf{j}} = \mathbf{C}^T \mathbf{j}$. It then follows that with the field redefinition in eq (B-2), the couplings to \tilde{B}_μ (the new hypercharge) are the same as in the original basis. After EWSB it is convenient to introduce the following fields:

$$\begin{pmatrix} \tilde{A}_\mu \\ \tilde{Z}_\mu \\ \tilde{Z}'_\mu \end{pmatrix} = \begin{pmatrix} \cos \theta_w & \sin \theta_w & 0 \\ -\sin \theta_w & \cos \theta_w & 0 \\ 0 & 0 & 1 \end{pmatrix} \begin{pmatrix} \tilde{B}_\mu \\ W_\mu^3 \\ \tilde{B}'_\mu \end{pmatrix} \quad (\text{B-3})$$

The \tilde{A}_μ field will have no mass terms since it couples to the generator $T_3 + Y$ by definition of the Weinberg angle ($U(1)_{EM}$ unbroken). The SM Higgs field couples to both the SM neutral

gauge boson and to B' , so after spontaneous symmetry breaking there will be mass mixing terms. In general, mass mixing terms still exist after going to the “tilde” basis:

$$\frac{1}{2} \begin{pmatrix} \tilde{Z}_\mu & \tilde{Z}'_\mu \end{pmatrix} \begin{pmatrix} m^2 & -\Delta \\ -\Delta & M^2 \end{pmatrix} \begin{pmatrix} \tilde{Z}^\mu \\ \tilde{Z}'^\mu \end{pmatrix} + W^+ W^- \text{ term.} \quad (\text{B-4})$$

The rotation necessary to diagonalise this mass matrix is parametrised by ζ as follows:

$$\begin{pmatrix} Z_- \\ Z_+ \end{pmatrix} = \begin{pmatrix} \cos \zeta & -\sin \zeta \\ \sin \zeta & \cos \zeta \end{pmatrix} \begin{pmatrix} \tilde{Z}^\mu \\ \tilde{Z}'^\mu \end{pmatrix} \quad (\text{B-5})$$

where Z_\pm are the mass and kinetic eigenstates, called the physical Z and Z' in the main text. With these relations one finds eq.(2) in the text for the transformation of the currents.

C Cross section formulae

We list here the partial decay rates and cross section formulae used to generate the limits presented in the text, Section 4. The interaction terms considered are parametrised below, with canonically normalised kinetic terms assumed:

$$ig_X Q_X \phi (\partial_\mu \phi^*) X^\mu + g_{XX'} v_\phi X^\mu X'_\mu \phi - g_X \bar{\psi} \gamma_\mu X^\mu (c_V - c_A \gamma_5)^X \psi + \text{h.c.} \quad (\text{C-1})$$

$$\text{where } g_{XX'} = \sqrt{2} g_X g_{X'} Q_{X(\phi)} Q_{X'(\phi)} \quad (\text{C-2})$$

where ϕ is a spin 0 field, $v_\phi = \sqrt{2}\langle\phi\rangle$, X^μ, X'^μ are gauge fields and $g_X, g_{X'}$ are the respective coupling constants. $Q_{X(\phi)}$ is the charge of the ϕ field under the symmetry whose gauge boson is X^μ and so on. The decay width of the Z' is an important quantity for any Z' mediated event close to the propagator pole. Some partial widths are given below, with the others assumed to be negligible. When relevant, the final state spin or polarisation configurations are summed over (but not for different colours).

$$\Gamma_{X \rightarrow f \bar{f}} = \frac{g_X^2 m_X}{12\pi} \sqrt{1 - \frac{4m_f^2}{m_X^2}} \left[(c_V^2)^X \left(1 + \frac{2m_f^2}{m_X^2} \right) + (c_A^2)^X \left(1 - \frac{4m_f^2}{m_X^2} \right) \right] \quad (\text{C-3})$$

$$\Gamma_{X \rightarrow \phi \phi^*} = \frac{g_X^2 m_X Q_{X(\phi)}^2}{48\pi} \left(1 - \frac{4m_\phi^2}{m_X^2} \right)^{3/2}$$

$$\begin{aligned}
\Gamma_{X \rightarrow W^+ W^-} &= \frac{g_X^2 m_X}{192 \pi} \left(1 - \frac{4m_W^2}{m_X^2}\right)^{3/2} \left(\frac{g_W^2 c_X^2}{g_X^2}\right) \left(\frac{m_X}{m_W}\right)^4 \left[1 + 20 \left(\frac{m_W}{m_X}\right)^2 + 12 \left(\frac{m_W}{m_X}\right)^4\right] \\
\Gamma_{X \rightarrow X' \phi} &= \frac{g_{XX'}^2 m_X}{192 \pi} \left(\frac{v_\phi^2}{m_{X'}^2}\right) \sqrt{1 - 2 \left(\frac{m_{X'}^2 + m_\phi^2}{m_X^2}\right) + \left(\frac{m_{X'}^2 - m_\phi^2}{m_X^2}\right)^2} \times \\
&\quad \left[1 + 2 \left(\frac{5 m_{X'}^2 - m_\phi^2}{m_X^2}\right) + \left(\frac{m_{X'}^2 - m_\phi^2}{m_X^2}\right)^2\right]
\end{aligned}$$

where $W^{3\mu} = c_X X^\mu + \dots$; $\left(W^{3\mu} = \sin \theta_w \tilde{A}^\mu + \cos \zeta \cos \theta_w Z_-^\mu + (-\sin \zeta \cos \theta_w) Z_+^\mu\right)$

C.1 Spin 0 dark matter

The parameters associated with the initial bosons are labelled (i), and those with the final states labelled (f). The tree level cross sections for annihilation via a vector boson are given to leading order in β_i , and are all p-wave annihilations:

- Dirac fermion anti-fermion product

$$\sigma = P \sqrt{1 - \frac{m_f^2}{m_i^2}} \left[(c_V^2 + c_A^2)_f^X + (c_V^2 - 2 c_A^2)_f^X \left(\frac{1}{2} \frac{m_f^2}{m_i^2} \right) \right] \quad (\text{C-4})$$

$$\text{where } P = \frac{g_X^4 (Q_X^2)_i}{(s - m_X^2)^2 + m_X^2 \Gamma_X^2} \left(\frac{s \beta_i}{12\pi} \right) \quad (\text{C-5})$$

- Spin 0, Spin 0 product

$$\sigma = P (Q_X^2)_f \frac{1}{4} \left(1 - \frac{m_f^2}{m_i^2} \right)^{3/2} \quad (\text{C-6})$$

- $W^+ W^-$ product

$$\sigma = P \left(1 - \frac{m_W^2}{m_i^2} \right)^{3/2} \left(\frac{g_W^2 c_X^2}{g_X^2} \right) \left(\frac{m_i}{m_W} \right)^2 \left[1 + \frac{3}{4} \left(\frac{m_W}{m_i} \right)^2 \right] \quad (\text{C-7})$$

- Gauge boson (X') and a scalar (ϕ) product

$$\begin{aligned} \sigma = & P \left(\frac{g_{XX'}^2}{g_X^2} \right) \sqrt{1 - \left(\frac{m_{X'}^2 + m_\phi^2}{2m_i^2} \right) + \left(\frac{m_{X'}^2 - m_\phi^2}{4m_i^2} \right)^2} \left[\frac{v_\phi^2}{32m_{X'}^2} \right] \\ & \times \left[2 + \left(\frac{5m_{X'}^2 - m_\phi^2}{m_i^2} \right) + \frac{1}{8} \left(\frac{m_{X'}^2 - m_\phi^2}{m_i^2} \right)^2 \right] \end{aligned} \quad (\text{C-8})$$

$$\text{where} \quad v_H^2 = \frac{4m_W^2}{g_W^2} \quad (\text{C-9})$$

$$v_\phi^2 = \left(\frac{m_{Z'} \cos \chi}{g' Q'_\phi} \right)^2 \left[1 - \frac{\Delta^2 \cos^2 \theta_w}{m_W^2 (m_{Z'}^2 - m_W^2 \sec^2 \theta_w)} \right] \quad (\text{C-10})$$

D Sommerfeld effect

In the following we provide more details about the Sommerfeld effect mentioned in Section 4. A more complete version of this study will appear elsewhere [47]. When the initial or final state of an interaction event involves slow moving particles, attractive or repulsive forces between these particles can lead to large enhancements or suppressions in the cross section compared to a perturbatively calculated result. This has long been known in nuclear physics and condensed matter physics as the Sommerfeld effect. Recently, its importance has been pointed out for cosmological calculations of thermal relics, and the indirect detection of dark matter [34, 35, 36, 37, 38, 39, 40].

The non-perturbative physics can be thought of as the limit of perturbative Feynman diagrams, with an infinite number of particle exchanges. For 2-body scattering this involves a “ladder” diagram. The solution of the non-perturbative vertex function, Γ , is given by the Bethe-Salpeter equation:

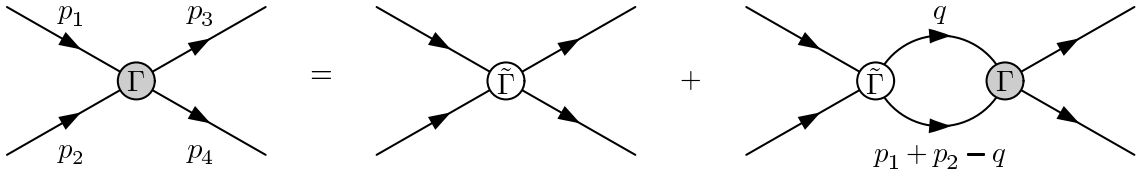


Figure D-i: Bethe-Salpeter equation in diagrammatic form.

$$i\Gamma(p_1, p_2; p_3, p_4) = i\tilde{\Gamma}(p_1, p_2; p_3, p_4) + \int \frac{d^4 q}{(2\pi)^4} \tilde{\Gamma} G(q) G(p_1 + p_2 - q) \Gamma \quad (\text{D-1})$$

where $\tilde{\Gamma}$ are “compact” vertices which do not involve any intermediate state composed solely of the scattering particles, and G is the non-perturbative propagator. The inhomogeneous integral equation for Γ can be solved to arbitrary accuracy, given that $\tilde{\Gamma}$ and the propagator are sufficiently well known from perturbative calculations. The finite ladders can be neglected when near the poles of the scattering states, which leads to the non-perturbative nature of this effect and a homogeneous integral equation. For an annihilation process as shown in Fig D-ii, the matrix element for the diagram with the ladder is related to the one without a ladder as given below:

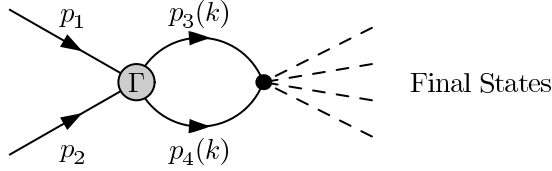


Figure D-ii: Diagram of Non-Perturbative Scattering before Annihilation

$$\begin{aligned} \mathcal{M}_{\text{with ladder}}(p_1, p_2; \{p_f\}) &= \int \frac{d^4 k}{(2\pi)^4} \mathcal{M}_{\text{w/o}}(p_3, p_4; \{p_f\}) G(p_3) G(p_4) \Gamma(p_1, p_2; p_3, p_4) \\ &= \int \frac{d^3 k}{(2\pi)^3} \mathcal{M}_{\text{w/o}}(\mathbf{k}, -\mathbf{k}; \{p_f\}) \tilde{\psi}_{\text{BS}}(\mathbf{k}), \end{aligned} \quad (\text{D-2})$$

where the Bethe-Salpeter wavefunction, $\tilde{\psi}_{\text{BS}}$, is introduced in the centre of momentum frame, and the intermediate scattering particles are taken on-shell. It follows that for non-relativistic processes, the Bethe-Salpeter wavefunction is equivalent to the solution of the Schrödinger equation with a potential that accounts for the scattering interactions [41]. For central potentials, the spherical harmonic basis is convenient for solving the Schrödinger equation:

$$\psi_{Elm}(\mathbf{r}) = R_{El}(r) Y_{lm}(\theta_r, \phi_r) \quad (\text{D-3})$$

The Fourier transform of eq (D-3) is determined below:

$$\begin{aligned}
\tilde{\psi}_{Elm}(\mathbf{k}) &= \int d^3r \psi_{Elm}(\mathbf{r}) e^{i\mathbf{k}\cdot\mathbf{r}} \\
&= \int r^2 dr \int d\Omega_r R_{El}(r) Y_{lm}(\theta_r, \phi_r) \left[\sum_{l'=0}^{\infty} \sum_{m'=-l'}^{l'} i^{l'} 4\pi j_{l'}(kr) Y_{l'm'}^*(\theta_r, \phi_r) Y_{l'm'}(\theta_k, \phi_k) \right] \\
&= Y_{lm}(\theta_k, \phi_k) \left[i^l 4\pi \int_0^{\infty} r^2 j_l(kr) R_{El}(r) dr \right] \\
&\equiv Y_{lm}(\theta_k, \phi_k) F_{El}(k)
\end{aligned} \tag{D-4}$$

It is therefore useful to decompose the matrix element in the same orthonormal momentum space basis to calculate eq (D-2). The weighting of the components of the Bethe-Salpeter wavefunction with different (l, m) quantum numbers is determined by the matrix element. If $\mathcal{M}_{w/o}$ is expressed as a polynomial in k , the result of integration of the wavefunction weighted by extra powers of k needs to be found. This can be done by considering derivatives of the position space radial wavefunction and the inverse Fourier transform relation:

$$R_{El}(r) = \frac{(-i)^l}{2\pi^2} \int_0^{\infty} k^2 j_l(kr) F_{El}(k) dk \tag{D-5}$$

$$\partial_r R_{El}(r) = \frac{(-i)^l}{2\pi^2} \int_0^{\infty} k^2 \partial_r [j_l(kr)] F_{El}(k) dk \tag{D-6}$$

Using a series expansion of the spherical Bessel function, then

$$\left. \frac{\partial^{l+2n} R_{El}(r)}{\partial r^{l+2n}} \right|_{r=0} = \frac{(l+2n)! (-1)^n}{2^n n! (2l+2n+1)!!} \frac{(-i)^l}{2\pi^2} \int_0^{\infty} k^2 k^{l+2n} F_{El}(k) dk \tag{D-7}$$

Suppose the full matrix element is dominated by the contribution of one term in $\mathcal{M}_{w/o} \propto k^{l+2n} Y_{lm}$, where n is some non-negative integer. In this case, the cross section which accounts for the ladder is related by an overall factor to the cross section calculated from diagrams without the ladder ($\sigma_{\text{with ladder}} = S_{l,n} \sigma_{w/o}$), valid in the non-relativistic limit. $S_{l,n}$ is called the Sommerfeld factor, with the value:

$$S_{l,n} = \left| \left(\frac{n! 2^n (2l+2n+1)!!}{(l+2n)! (M\beta)^{l+2n}} \right) \frac{\partial^{l+2n} R_{El}(r)}{\partial r^{l+2n}} \right|_{r=0}^2 \tag{D-8}$$

It is common to ignore the effect present for non-zero angular momentum processes, arguing that the angular momentum barrier always suppresses higher partial wave processes. However, if s-wave interactions are small compared to higher partial wave processes, as when scalars annihilate via a heavy vector, this argument is not always applicable.

D.1 Coulomb potential

The reduced Schrödinger radial equation for a two-body system of particles each with mass M , and a Coulomb potential is as follows:

$$\left(\frac{\partial_r^2}{M} + M\beta^2 + \frac{A}{r} - \frac{l(l+1)}{Mr^2} \right) r R_l(r; M, A, \beta) = 0 \quad (\text{D-9})$$

where β is the speed of each particle when at infinite separation in the centre of mass frame. This can be re-written in terms of dimensionless variables:

$$\left(\partial_z^2 + \frac{1}{4} + \frac{x}{2z} - \frac{l(l+1)}{z^2} \right) z R_l(z; x) = 0 \quad \text{where} \quad z = 2rM\beta \quad x = A/\beta \quad (\text{D-10})$$

The solutions are given in terms of a confluent hypergeometric function:

$$R_l(z; x) = e^{\pi x/4} e^{-iz/2} z^l \frac{\Gamma(1 + \frac{ix}{2} + l)}{(2l+1)!} {}_1F_1 \left(1 + \frac{ix}{2} + l, 2l+2, iz \right) \quad (\text{D-11})$$

$$= e^{\pi x/4} e^{-iz/2} z^l \sum_{j=0}^{\infty} \left[\frac{\Gamma(1 + \frac{ix}{2} + l + j)}{(2l+1+j)!} \frac{(iz)^j}{j!} \right] \quad (\text{D-12})$$

The Sommerfeld factor written in this dimensionless formulation is:

$$S_{l,0} = \left| \frac{(2l+1)!}{(l!)^2} \frac{\partial^l R_l(z)}{\partial z^l} \right|_{z=0}^2 \quad (\text{D-13})$$

The result for non-zero angular momentum states due to Coulomb interactions is thus:

$$S_{l,0} = S_{0,0} \times \prod_{b=1}^l \left(1 + \frac{x^2}{4b^2} \right) \quad \text{where} \quad S_{0,0} = \frac{\pi x}{1 - e^{-\pi x}} \quad (\text{D-14})$$

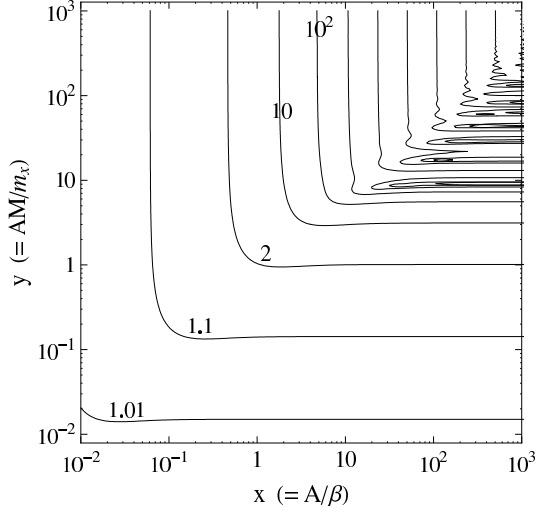
In a perturbative expansion, higher partial waves are suppressed by factors of β^2 . However, in the limit of small velocities (large x) the Sommerfeld factor for a Coulomb interaction fixes each partial wave to have the same velocity dependence.

D.2 Yukawa potential

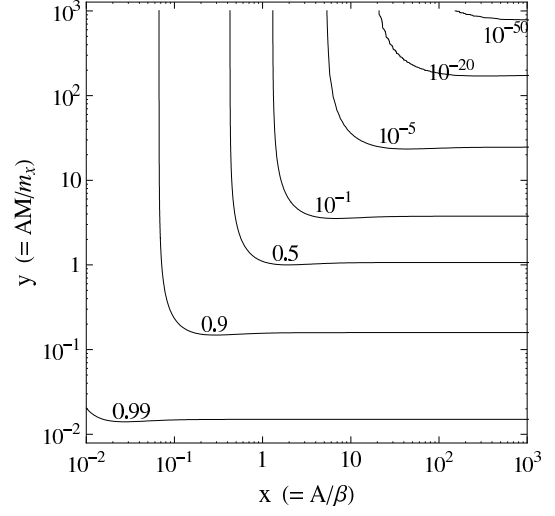
The Schrödinger equation with a Yukawa potential is related to the Coulomb case as follows:

$$A \rightarrow A e^{-m_X r} = A e^{-xz/(2y)} \quad \text{where} \quad y = AM/m_X \quad (\text{D-15})$$

where m_X is the mass of the mediator. The Sommerfeld factor for the $l = 0$ case has been presented by Cirelli, Strumia and Tamburini [38]. Figure D-iii shows the $l = 1$ case ($n=0$), where numerical simulations have been used to find the wavefunction.



(a) Attractive Potential



(b) Repulsive Potential

Figure D-iii: Sommerfeld Factor for Yukawa interaction of a p-wave state (contours not labelled vary by a factor of 10)

For small y , the Sommerfeld factor gets closer to unity as the angular momentum increases. This is because as the interaction is screened beyond some short distance, the increased angular momentum barrier becomes more efficient at keeping the wavefunction away from this core. For a repulsive Yukawa interaction, there is then less suppression for the higher partial waves. So, although higher partial waves may be neglected at a perturbative level, this ladder effect could cause them to become significant or even dominant. However, for attractive interactions, the larger angular momentum processes are enhanced less, so higher partial wave terms which are negligible in the perturbative expansion stay negligible.

There is always some reduction in the velocity dependent factor of the partial wave cross sections, in going to higher partial waves for non-zero β , but the $\beta^{2\Delta_l}$ suppression is only found for large velocities. For the attractive Yukawa potential, $l = 1$ bound states exist when $y \gtrsim 9.08$. The system can be close to the Breit-Wigner tails of these resonances when the relative velocity is small, and the Sommerfeld factor reflects this. In the limit $y \rightarrow \infty$, the Coulomb potential is approached, so the discussion in the previous subsection is relevant.

References

- [1] O. Adriani *et al.*, “Observation of an anomalous positron abundance in the cosmic radiation,” arXiv:0810.4995 [astro-ph].
- [2] J. Chang *et al.*, “An Excess Of Cosmic Ray Electrons At Energies Of 300.800 Gev,” Nature **456**, 362 (2008).
- [3] M. J. Strassler and K. M. Zurek, “Echoes of a hidden valley at hadron colliders,” Phys. Lett. B **651**, 374 (2007) [arXiv:hep-ph/0604261].
- [4] M. J. Strassler and K. M. Zurek, “Discovering the Higgs through highly-displaced vertices,” Phys. Lett. B **661**, 263 (2008) [arXiv:hep-ph/0605193].
- [5] M. J. Strassler, “Possible effects of a hidden valley on supersymmetric phenomenology,” [arXiv:hep-ph/0607160].
- [6] T. Han, Z. Si, K. M. Zurek and M. J. Strassler, “Phenomenology of Hidden Valleys at Hadron Colliders,” JHEP **0807**, 008 (2008) arXiv:0712.2041 [hep-ph].
- [7] M. J. Strassler, “Why Unparticle Models with Mass Gaps are Examples of Hidden Valleys,” arXiv:0801.0629 [hep-ph].
- [8] M. J. Strassler, “On the Phenomenology of Hidden Valleys with Heavy Flavor,” arXiv:0806.2385 [hep-ph].
- [9] H. P. Nilles, “Supersymmetry, Supergravity And Particle Physics,” Phys. Rept. **110** (1984) 1; S. Ferrara, L. Girardello and H. P. Nilles, “Breakdown Of Local Supersymmetry Through Gauge Fermion Condensates,” Phys. Lett. B **125** (1983) 457. H. P. Nilles, “Dynamically Broken Supergravity And The Hierarchy Problem,” Phys. Lett. B **115** (1982) 193. M. Dine, R. Rohm, N. Seiberg and E. Witten, “Gluino Condensation In Superstring Models,” Phys. Lett. B **156** (1985) 55. J. P. Derendinger, L. E. Ibanez and H. P. Nilles, “On The Low-Energy $D = 4$, $N=1$ Supergravity Theory Extracted From The $D = 10$, $N=1$ Superstring,” Phys. Lett. B **155** (1985) 65.
- [10] L. E. Ibanez and G. G. Ross, “Discrete gauge symmetry anomalies,” Phys. Lett. B **260** (1991) 291.

- [11] F. Wilczek, “A constructive critique of the three standard systems,” Czech. J. Phys. **54** (2004) A415 [arXiv:hep-ph/0401126].
- [12] R. Schabinger and J. D. Wells, “A minimal spontaneously broken hidden sector and its impact on Higgs boson physics at the Large Hadron Collider,” Phys. Rev. D **72** (2005) 093007 [arXiv:hep-ph/0509209].
- [13] B. Patt and F. Wilczek, “Higgs-field portal into hidden sectors,” [arXiv:hep-ph/0605188].
- [14] T. Hur, D. W. Jung, P. Ko and J. Y. Lee, “Electroweak symmetry breaking and cold dark matter from hidden sector technicolor interaction,” arXiv:0709.1218 [hep-ph].
- [15] D. G. Caldi, “Quark Mass Generation By Instantons,” Phys. Rev. Lett. **39** (1977) 121.
- [16] K. S. Babu, C. F. Kolda and J. March-Russell, “Leptophobic U(1)’s and the $R_b - R_c$ Crisis,” Phys. Rev. D **54** (1996) 4635 [arXiv:hep-ph/9603212].
- [17] K. S. Babu, C. F. Kolda and J. March-Russell, “Implications of generalized Z Z’ mixing,” Phys. Rev. D **57**, 6788 (1998) [arXiv:hep-ph/9710441].
- [18] See for example A. V. Manohar, “Large N QCD,” arXiv:hep-ph/9802419.
- [19] P. Di Vecchia and G. Veneziano, “Chiral Dynamics In The Large N Limit,” Nucl. Phys. B **171** (1980) 253.
- [20] G. ’t Hooft, “How Instantons Solve the U(1) Problem,” Phys. Rept. **142** (1986) 357.
- [21] J. E. Kim, G. Carosi, “Axions and the Strong CP Problem,” arXiv:0807.3125 [hep-ph].
- [22] A. Pich, “Chiral perturbation theory,” Rept. Prog. Phys. **58** (1995) 563 [arXiv:hep-ph/9502366].
- [23] B. Murakami, “The impact of lepton-flavor violating Z’ bosons on muon g-2 and other muon observables,” Phys. Rev. D **65** (2002) 055003 [arXiv:hep-ph/0110095].
- [24] D. C. Kennedy and B. W. Lynn, “Electroweak Radiative Corrections with an Effective Lagrangian: Four Fermion Processes,” Nucl. Phys. B **322** (1989) 1.
- [25] W. M. Yao *et al.* [Particle Data Group], “Review of particle physics,” J. Phys. G **33**, 1 (2006).

- [26] T. Aaltonen *et al.* [CDF Collaboration], “Search for new physics in high mass electron-positron events in $p\bar{p}$ collisions at $\sqrt{s} = 1.96\text{-TeV}$,” Phys. Rev. Lett. **99**, 171802 (2007) arXiv:0707.2524 [hep-ex] FERMILAB-PUB-07-367-E.
- [27] C. Ciobanu, T. Junk, G. Veramendi, J. Lee, G. De Lentdecker, K. McFarland, K. Maeshima [CDF Collaboration] “Z’ generation with PYTHIA” Fermilab-FN-0773-E
- [28] D. Feldman, Z. Liu and P. Nath, “Probing a very narrow Z’ boson with CDF and D0 data,” Phys. Rev. Lett. **97** (2006) 021801 [arXiv:hep-ph/0603039].
- [29] D. Feldman, Z. Liu and P. Nath, “The Stueckelberg Z prime at the LHC: Discovery potential, signature spaces and model discrimination,” JHEP **0611** (2006) 007 [arXiv:hep-ph/0606294].
- [30] D. Feldman, B. Kors and P. Nath, “Extra-weakly interacting dark matter,” Phys. Rev. D **75** (2007) 023503 [arXiv:hep-ph/0610133].
- [31] D. Feldman, Z. Liu and P. Nath, “The Stueckelberg Z’ extension with kinetic mixing and milli-charged dark matter from the hidden sector,” Phys. Rev. D **75** (2007) 115001 [arXiv:hep-ph/0702123].
- [32] D. Feldman, Z. Liu and P. Nath, “The Stueckelberg Extension and Milli Weak and Milli Charge Dark Matter,” AIP Conf. Proc. **939** (2007) 50 arXiv:0705.2924 [hep-ph].
- [33] M. Cvetič and S. Godfrey, “Discovery and identification of extra gauge bosons,” [arXiv:hep-ph/9504216].
- [34] A. Sommerfeld, “Über die Beugung und Bremsung der Elektronen,” Ann. Phys. **403** (1931) 257
- [35] J. Hisano, S. Matsumoto and M. M. Nojiri, “Explosive dark matter annihilation,” Phys. Rev. Lett. **92** (2004) 031303 [arXiv:hep-ph/0307216].
- [36] J. Hisano, S. Matsumoto, M. M. Nojiri and O. Saito, “Non-perturbative effect on dark matter annihilation and gamma ray signature from galactic center,” Phys. Rev. D **71** (2005) 063528 [arXiv:hep-ph/0412403].

- [37] J. Hisano, S. Matsumoto, M. Nagai, O. Saito and M. Senami, “Non-perturbative effect on thermal relic abundance of dark matter,” *Phys. Lett. B* **646** (2007) 34 [arXiv:hep-ph/0610249].
- [38] M. Cirelli, A. Strumia and M. Tamburini, “Cosmology and Astrophysics of Minimal Dark Matter,” *Nucl. Phys. B* **787** (2007) 152 arXiv:0706.4071 [hep-ph].
- [39] J. March-Russell, S. M. West, D. Cumberbatch and D. Hooper, “Heavy Dark Matter Through the Higgs Portal,” *JHEP* **0807**, 058 (2008) arXiv:0801.3440 [hep-ph].
- [40] J. D. March-Russell and S. M. West, “WIMPonium and Boost Factors for Indirect Dark Matter Detection,” arXiv:0812.0559 [astro-ph].
- [41] V. B. Berestetskii, E. M. Lifshitz and L. P. Pitaevskii, “Quantum Electrodynamics,” Oxford, UK: Pergamon (1982) 652 P. (Course Of Theoretical Physics, 4)
- [42] M. Drees, H. Iminniyaz and M. Kakizaki, “Constraints on the very early universe from thermal WIMP dark matter,” *Phys. Rev. D* **76** (2007) 103524 arXiv:0704.1590 [hep-ph].
- [43] G. Hinshaw *et al.* [WMAP Collaboration], “Five-Year Wilkinson Microwave Anisotropy Probe (WMAP) Observations: Data Processing, Sky Maps, and Basic Results,” arXiv:0803.0732 [astro-ph].
- [44] K. Griest and M. Kamionkowski, “Unitarity Limits on the Mass and Radius of Dark Matter Particles,” *Phys. Rev. Lett.* **64**, 615 (1990).
- [45] K. Griest and D. Seckel, “Three exceptions in the calculation of relic abundances,” *Phys. Rev. D* **43**, 3191 (1991).
- [46] B. W. Lee and S. Weinberg, “Cosmological lower bound on heavy-neutrino masses,” *Phys. Rev. Lett.* **39**, 165 (1977).
- [47] S. Cassel, work in progress.